Investigation on Induced Intra/Interlaminar Damage Propagation in CFRP Subjected to Cyclic Tensile Loading After Impact (TAI)

Francisco Maciel Monticeli[1,2(✉)], Felipe Ruivo Fuga[2], Mariano Andrés Arbelo[2], and Maurício Vicente Donadon[2]

[1] Department of Aerospace Structure Materials, Faculty of Aerospace Engineering, Kluyverweg 1, 2629HS Delft, Netherlands
F.M.Monticeli@tudelft.nl

[2] Department of Aeronautical Engineering, Technological Institute of Aeronautics (ITA), São José Dos Campos 12228-615, Brazil

Abstract. Impact damage to composite structures results in multiple, complex failure modes, often requiring the replacement of entire components and thereby escalating aircraft maintenance costs. To address this issue, the present study investigates the damage propagation behaviour with particular emphasis on intra- and interlaminar failure modes. Carbon fibre/epoxy composites were subjected to tensile after impact (TAI) fatigue tests at different energy levels to induce different damage modes and extents within the specimens. A non-destructive testing technique (C-scan) was used to assess the interlaminar damage propagation, while the intralaminar fracture toughness of the post-impact specimens was characterised using a finite fracture mechanics model. The results show that the crack propagation behaviour is strongly influenced by the initial impact damage characteristics, in particular the impact energy level. Lower impact energies tend to promote interlaminar failure modes leading to fatigue crack propagation by delamination. Conversely, higher impact energy levels induce fibre fracture, resulting in a self-similar relationship between intra- and interlaminar propagation.

Keywords: Fatigue · Crack Propagation · Finite Fracture Mechanics · Polymer Composite

1 Introduction

The progressive adoption of carbon fibre-reinforced polymer (CFRP) composites in the aeronautic and aerospace fields has led to a substantial weight reduction while ensuring optimal correlation with mechanical properties [1, 2]. This remarkable increase in structural application underscores its significance as a transformative material in achieving lightweight design objectives without compromising structural integrity [3].

Structural components within aircraft are designed to withstand the load per established airworthiness regulations [4]. Nevertheless, unexpected structural damage can compromise the stability of these components [5]. Such damage leads to a decay in

H. Altenbach et al. (Eds.): CAMPE 2023, pp. 227–236, LNME 2025.
https://doi.org/10.1007/978-3-031-82979-6_23

mechanical properties, rendering the component incapable of supporting the projected load. Aeronautical structures may be subjected to different impact scenarios whilst in service, including bird strikes and hail (impact damages), which can significantly affect the composite mechanical behaviour [6, 7]. Allan [8] also conducted a comprehensive study revealing that the repair or replacement costs of primary and secondary structures subject to bird strike-induced damage can reach US$ 1.2 billion annually. Moreover, impact damage initiates intra- and interlaminar fractures, further amplifying the complexity of analysing and controlling the damage progression.

The interlaminar fracture refers to the separation or delamination between adjacent layers of composite material [8]. Intralaminar fracture refers to fractures that begin and grow within each layer, and translaminar fracture of fibres should also be considered [9]. Measuring and distinguishing damage propagation induced by fatigue loading, particularly interlaminar and translaminar failure modes, imposes challenges for designing and inspecting composite aerostructures. Traditional non-destructive evaluation techniques may need help differentiating between these fracture types, as their resolution often falls short in detecting smaller-scale damage [10, 11]. Furthermore, the complex mechanisms involved in damage propagation within composite materials, including delamination and fractures within layers, demand advanced experimental techniques and physical-based models [12, 13].

Multi-scale damage further complicates the measurement of fatigue damage propagation [14]. Microcracks, matrix cracks, fibre breaks, and their interactions can occur simultaneously, demanding a comprehensive approach that combines several experimental techniques [15, 16]. Overcoming the challenges in distinguishing interlaminar and intralaminar damage provides a crucial advantage in effectively controlling the fatigue life of a structural component aiming at designing damage-tolerant structures.

In the search to comprehensively characterise the physical behaviour of crack propagation in laminated composites, a lack of current knowledge has been identified regarding the simultaneous consideration of intra/interlaminar fractures in crack propagation rate to assess the energy release during cyclic loading. Therefore, this work aims to investigate the behaviour of intra/interlaminar damage propagation in structural composites by subjecting them to post-impact cyclic tensile stress (TAI – tensile after impact). Additionally, the assessment of damage propagation will be conducted using a non-destructive testing technique (ultrasound microscopy) combined with the finite fracture mechanic model.

2 Experimental Procedure

2.1 Materials and Manufacturing

The composite laminate was manufactured by resin transfer moulding (RTM). The reinforcement used was carbon fibre plain weave fabrics, Hexcel® HexForce™ AGP193-P. The matrix was epoxy resin (Araldite® LY 5052) with a 100:32 weight ratio with hardener (Aradur® 5052). The stacking sequence was a quasi-isotropic lay-up configuration with eight layers $[0/45/-45/90]_s$. The laminate thickness was 2 mm, with eight layers of reinforcement (50% of fibre/matrix). The manufacturing procedure involved injecting resin at 5 bar injection pressure at 25 °C for 120 min. The 20 mbar vacuum was applied

during injection. The cure was carried out at 25 °C for 24 h and then a post-cure at 100 °C for 4 h.

2.2 Experimental Test Configurations

The low-velocity impact (LVI) tests were performed according to the ASTM D7136M-15 standard, where a specimen geometry of 200 × 110 × 2 mm^3 was chosen, and a 1.46 kg semi-hemispherical impactor with 16 mm diameter was used. The impactor was dropped from a specific height and guided by lateral rails. The drop heights were set to achieve impact energy levels of 11 and 18 J. Detailed test information can be found in Ref. [16].

Tensile testing was carried out using an MTS servo-hydraulic machine with a 250 kN load cell. The static tests were conducted at a rate of 2 mm/min. The specimen dimensions were 200 × 50 × 2 mm^3, with the impact damage at the central region of the specimen. The fatigue tests were performed under load control with a sinusoidal loading spectrum with a maximum stress amplitude of 85% of the laminate tensile strength (σ_{max}) and stress ratio R = ($\sigma_{min}/\sigma_{max}$) = 0.1 and frequency of 5 Hz. A constant amplitude was maintained during the fatigue tests. The elastic properties at ply level are $E_1 = E_2 =$ 51.83 GPa, $G_{12} = 2.82$ GPa, $v_{12} = 0.064$, measured following ASTM D3039 and ASTM D3518 standards. C-scan images were obtained through acoustic ultrasound inspection using the Sonotron ISONIC 2006 (NDT, 2006) equipment with a 5 MHz probe.

Figure 1 illustrates the flowchart of each test step and the data analysis during each stage. Initially, impact tests were conducted at two distinct impact energy levels. Subsequently, a static tensile test was performed to evaluate the rupture stress corresponding to each impact energy level. For additional specimens, tensile tests were applied through cyclic loading, with intervals between cycles to facilitate C-scan analysis. Following 100,000 cycles, a static stress-to-fracture test was performed to determine the new post-fatigue rupture residual stress. The remote stress is the failure stress measured during the static test. Remote stress was measured for the pristine material (laminate without damage), after impact, and after impact and tensile cyclic loading. All collected data were analysed utilising the finite fracture mechanics (FFM) model, as proposed by Camanho et al. [14], which accounts for open-hole strength and follows Eqs. 1 and 2, which can be fully described in the supplementary material (Eqs. S1–S12) and also in Ref. [14]. The application of this methodology primarily involves assessing the crack propagation rate (dL/dN) relative to the released energy (ΔK) per cycle. In parallel, interlaminar growth analyses were conducted using C-scan techniques, recognising that the FFM model neglected the propagation of interlaminar damage.

$$\frac{1}{L}\int_{R}^{R+L} \sigma_{yy}(x,0)dx = X_t(N); \text{ for } X_t = X_t(N) = C_1 N^{-m_1} \tag{1}$$

$$\frac{1}{L}\int_{R}^{R+L} K_I^2(a)da = K_I^2(N); \text{ for } K_I = K_I(N) = C_2 N^{-m_2} \tag{2}$$

where, L is the crack size at the failure, R is the hole radius ($2R = D$), $\sigma_{yy}(x,0)$ is stress distribution along the *x-axis*, X_t is the strength of the laminate without damage, K_{IC} is

the mode I intralaminar fracture toughness of the laminate, N is the cycle number, C_i and m_i are the constants coefficients. The remote and pristine stresses represent the failure stress of the material. The pristine stress is the failure stress of the material without impact damage, and the remote stress means the failure stress after impact and fatigue damage added to the material.

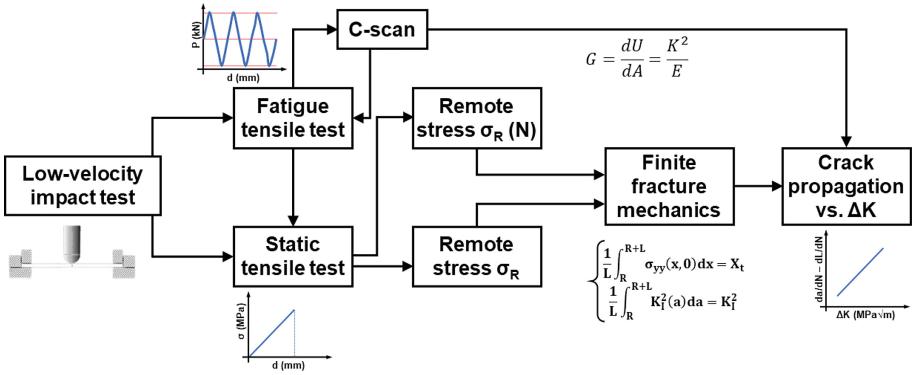

Fig. 1. Work flowchart following test procedure and data analysis.

3 Results and Discussion

Table 1 presents the summarised results of the experimental drop test, divided into low-energy (LE) and high-energy (HE) groups. Considering the impact mass and the standard procedure, the heights used were 76.58 and 125.32 cm to reach 11 and 18 J, respectively. The velocity at the impact (v_i) provides insight into the initial kinetic energy the impacting object possesses. On the other hand, v_{out} represents the impactor velocity after the collision, which was determined by analysing the rebound or post-impact motion of the impactor. The energy associated with the incident impact (E_i) was calculated using the mass and velocity of the impactor. It represents the total kinetic energy transferred to the specimen during the collision. The dissipated energy (E_d) quantifies the amount of energy absorbed and dissipated by the specimen due to the impact.

The difference in incidence velocities is attributed to variations in the positioning height of the impactor and friction effects. The output velocity corresponds to the dissipated energy within the material. Consequently, the low-energy (LE) level exhibits relatively lower energy dissipation due to induced internal delamination fractures and a limited occurrence of intralaminar fractures (Fig. 2b - 11J). On the other hand, samples subjected to higher impact energy levels (HE) increase the energy dissipation, characterised by the difference between the incident and rebound velocities. This disparity arises from the greater extent of material fracture resulting from the higher impact energy level (Fig. 2b - 18J), consuming more energy in the process.

Post-impact cyclic stress loading was applied after subjecting the laminate to impact at two levels of impact energy. Figure 2a exhibits the C-scan images of non-impacted

Table 1. Experimental impact results

Impact energy	v_i (m . s^{-1})	v_{out} (m • s^{-1})	E_i (J)	E_d (J)
Low (LE)	3.88 ± 0.03	2.77 ± 0.14	11.00 ± 0.17	5.43 ± 0.42
High (HE)	4.96 ± 0.08	2.69 ± 0.15	17.96 ± 0.36	12.71 ± 0.26

laminate and the impacted curve with respective C-scan images from each impact damage energy. Figure 2b shows the images of the backside of the impacted laminate and the ultrasound results after cyclic loading. Similar behaviour can be observed in both impact tests, where the maximum load reaches approximately 3000 N in both cases. However, a significant difference is observed in Table 1, indicating longer contact with the impactor for higher impact energy levels (HE), resulting in more intralaminar damage. Conversely, the low-energy (LE) laminates primarily exhibited internal damage, particularly associated with delamination. The results presented are consistent with published studies [16, 17] showing delamination as the primary fracture mechanism at low impact energy and increased fibre fracture at higher impact energy.

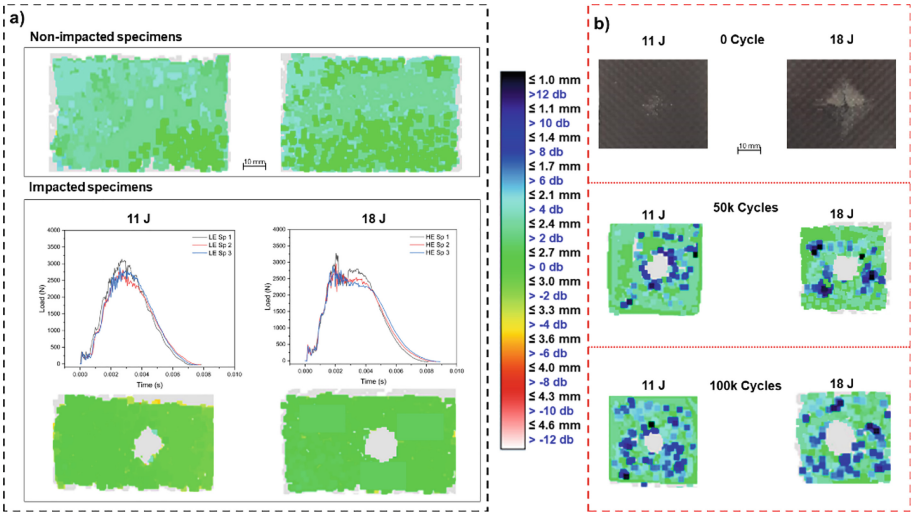

Fig. 2. Mechanical test analysis: a) impact test curve and C-scan images, and b) propagation of interlaminar fatigue damage (C-scan images).

The regions surrounding the hole after cyclic loading displayed fluctuations in attenuation values. This phenomenon can be attributed to internal damage. Ultrasound waves are emitted through the thickness, travel through the material and return to the receiving probe. In case of internal defect, there is attenuation/loss of the return signal, generating a change in the colour scale to identify internal damages. As a result, the wave direction deviates, leading to variations in the signal read by the probe.

During the cyclic loading of impacted samples, the crack initiates in the matrix and propagates along the fibre/matrix interface, following the fibre direction and forming splitting [18]. The static test promotes intralaminar fractures perpendicular to the fibre direction, reaching the required energy for fibre rupture. On the other hand, splitting and microcracking damage generate a preference for interlaminar propagation occurring between the laminae since fatigue loading provides sufficient energy for these fracture patterns. Interlaminar fractures can grow and lead to significant stress decay, potentially preventing translaminar fractures in the material [19]. Therefore, C-scan ultrasound images were used to measure the propagation of interlaminar damage after the cyclic loading. The increase in fracture radius was evaluated by considering the equivalent fracture area generated by the highlighted fluctuations in attenuation values associated with the equivalent delamination region, as shown in Fig. 2b.

After the cyclic test, a static tensile test was performed in the same specimen to evaluate the residual stress. According to Eqs. 1 and 2, as there is a decay on the remote stress resulting from the fatigue damage, the size of the crack length (L) also changes. Table 2 presents the experimental results of the static and cyclic tests (as shown in flowchart Fig. 1). The C-scan damaged radius is the internal damaged area (interlaminar), measured in terms of the equivalent radius with the C-scan images through the thickness, following Fig. 2b. L is the translaminar crack length provided from Eqs. 1 and 2. The static test after fatigue provided the remote stress (σ_r), considered the fracture stress. K_I was calculated following $K_I = \sigma F_1 F_2 \sqrt{\pi a}$, in which F_i are the corrections factor (detailed described in Eqs. S8 and S9 in the supplementary material), σ is the remoted measured stress, and a is the total crack size (open-hole radius R + crack length L).

Table 2. Experimental results of damage propagation for low and high impact energies.

Low-energy (LE)					
C-scan damage radius (mm)	L (mm)	σ_r (MPa)	Cycles ($\times 10^3$)	K_I (MPa$\sqrt{}$m)	X_t (MPa)
0	3.97	443.28	0	58.70	497.99
3.56	4.50	441.18	50	86.69	
12.81	4.89	431.93	100	96.20	
High-energy (HE)					
C-scan damage radius (mm)	L (mm)	σ_r (MPa)	Cycles ($\times 10^3$)	K_I (MPa$\sqrt{}$m)	X_t (MPa)
0	2.71	430.80	0	56.56	497.99
4.54	4.87	414.37	50	89.84	
9.28	5.04	402.17	100	101.18	

The pristine stress (X_t) was measured from a non-impacted in the same lay-up configuration. The HE impact provides a diameter of 20 mm, and the LE impact provides a damage diameter of 10 mm. After cyclic loading, the LE exhibits larger internal damage

growth than the HE laminates, considering the delamination measured by the C-scan. HE presents lower damage propagation through delamination due to translaminar damage from L-crack growth. The low coefficient of variation presented ($\approx 3.74\%$) indicates that the specimen exhibited homogeneity behaviour. Therefore, the average values will be used to model finite fracture mechanics. The relationship between the results in Table 2 is observed in detail in Fig. 3.

The residual stress exhibits a decay as a function of cycles (Fig. 3a). The HE specimens exhibited a more abrupt stress decay than the LE specimens, indicating a dependency on the initial damage generated by the impact test. Along the cycles, the stress decay difference is 6.6% for the high-energy laminate, while for the low-energy laminate, it is 2.5%. This difference is directly associated with the initial decay generated by the impact fracture. In other words, HE specimens have a larger fracture region (i.e., 20 mm) and tend to show higher stress decay during cyclic loading than LE specimens, which present 10 mm of the fractured area.

The propagation of simultaneous intra/interlaminar damage is directly associated with the impact energy level. Even with the delamination present for both energy levels, significant intralaminar fracture only occurs for higher energy. Delamination is crucial in fatigue fracture analysis [20]. The interfacial region between plies is highly susceptible to delamination mechanisms due to its weaker mechanical and chemical interaction than fibre rupture. Consequently, microcracking between layers during cyclic loading can reduce stress [21]. Therefore, this work focused on measuring interlaminar damage progression through damage growth (C-scan) and intralaminar propagation (FFM model).

The crack growth (da) was considered analogous to the crack length (L) in the FFM model and the radius size (R) of the internal damage region measured by the *C-scan*. Consequently, the crack growth curve was determined by the derivative of the curve in Fig. 3b for each fracture mechanism concerning the number of cycles following the Paris curve model [22]. Figure 3b illustrates the growth rate of interlaminar and intralaminar damages as a function of cycles for each post-impact energy level. A significant increase in interlaminar crack growth is observed for the LE specimen, while the intralaminar (translaminar) crack growth presents a lower propagation. This difference arises because low-impact energy results in more damage between layers and less fibre breakdown [16]. The interlaminar damage propagation during the application of cyclic loading is more prominent for the LE specimen, leading to a non-significant stress decay. Consequently, there is a lower variation in the crack length (L) since it is directly proportional to the stress variation.

The HE specimen exhibits a higher initial rate of intralaminar damage growth. This is attributed to the higher energy impact-induced fracture, resulting in a higher fraction of fibre rupture and a larger fractured region than LE. Thus, the growth of interlaminar and intralaminar damage occurs in parallel behaviour, as the impact damage establishes a similar relationship between both types of damage, promoting parallel growth for both failure modes. These results suggest that the propagation and failure modes are influenced by the initial configuration of the impact damage [23].

Based on the experimental data presented in Fig. 3c, a second-order polynomial curve was fitted to each experimental data. Subsequent, those curves were used to develop the

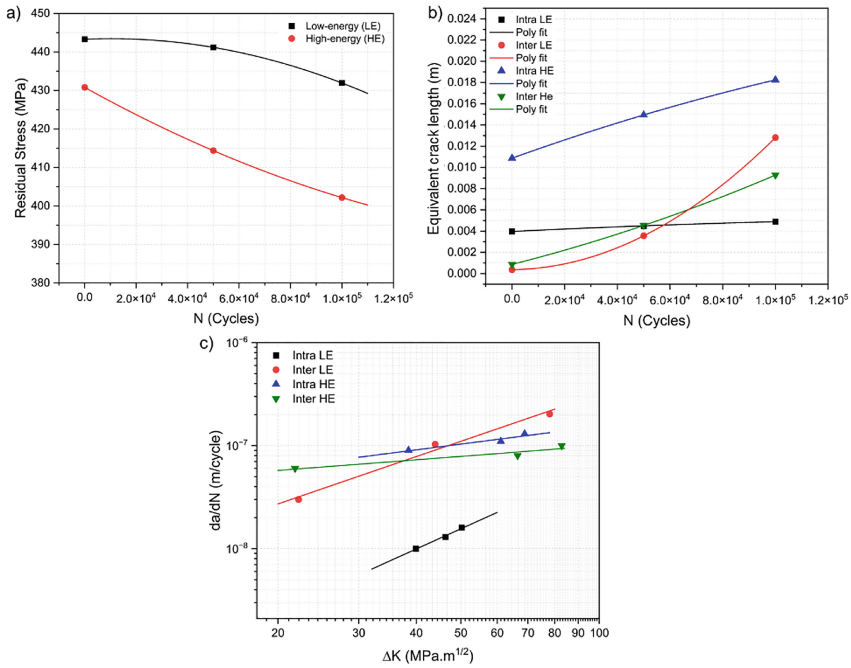

Fig. 3. a) SN curve, b) Compliance curve: equivalent crack length vs. cycles, and c) Paris curve: crack propagation rate versus stress intensity factor.

crack growth rate curve (*da/dN*), which was considered analogous to the crack growth rate of size *L* (*dL/dN*), as well as the growth of the internal damage radius *R* (*dR/dN*). The stress intensity factor (*K*) was calculated using Eq. 2.

Figure 3c shows the curves based on the power law curve, in which the crack propagation rate is related to the stress intensity factor (SIF – ΔK) as a similitude energy parameter. The following equation describes the crack propagation behaviour for each case: $\mathrm{LE}_{\mathrm{intra}}\ (da/dN) = 6 \times 10^{-12}(\Delta K)^{2.01}$; $\mathrm{LE}_{\mathrm{inter}}\ (da/dN) = 9 \times 10^{-12}(\Delta K)^{2.35}$; $\mathrm{HE}_{\mathrm{intra}}\ (da/dN) = 2 \times 10^{-8}(\Delta K)^{0.47}$, $\mathrm{HE}_{\mathrm{inter}}\ (da/dN) = 2 \times 10^{-8}(\Delta K)^{0.34}$. After interpolating the experimental data to determine the average crack propagation behaviour, the power function fitting coefficients C_i and m_i for each damage mode.

A comparative analysis of failure modes shows that the LE specimen exhibits lower intralaminar crack propagation rate levels, mainly due to the delamination-induced impact damage, favouring interlaminar propagation. In addition, the angular coefficient for interlaminar damage (2.35) is higher than that for intralaminar damage (2.01), suggesting that intralaminar damage suffers a more abrupt propagation than interlaminar propagation.

In contrast, the HE specimen demonstrates a similar behaviour between the two curves, indicating a close relationship between the propagation region for intra and interlaminar failure modes. The values of the constants for each curve support this observation. The damage caused by the initial impact directly affects the crack propagation under cyclic loading [24, 25]. In other words, lower impact energy levels result in a higher

crack propagation rate of interlaminar fracture, making delamination more susceptible to growth during cyclic loading. Higher impact energy leads to more intralaminar initial damage features, creating an equal propagation behaviour for both modes.

4 Conclusion

The Tensile After Impact (TAI) fatigue test was conducted to investigate the damage propagation behaviour and the effects of different impact energy levels in carbon fibre/epoxy composites. Intra- and interlaminar crack propagation were measured and analysed using non-destructive ultrasonic techniques and a finite fracture mechanics model. A failure envelope based on the Paris model was derived by establishing a correlation between the different damage modes and the crack propagation rate.

The results show that the crack propagation behaviour is directly influenced by the amount and type of initial damage, which is determined by the impact energy level. In particular, damage zones caused by low energy impacts lead to a more rapid absolute increase in interlaminar cracking. As the severity of the impact damage increases, there is a shift in the initial failure modes, indicating a synergistic interaction between intra- and interlaminar failure mechanisms. Consequently, higher impact energy levels promote a parallel propagation rate for intra- and interlaminar fractures, highlighting the relationship between damage severity and crack propagation dynamics.

Acknowledgements. The authors acknowledge financial support from FAPESP (process number: 2021/05706-5), CNPq (process number: 301069/2019-0) and CAPES (financial code 001).

References

1. Shesan, Q., Stephan, A., Chioma, A., Neerish, R., Rotimi, S. Fiber-matrix relationship for composites preparation. Book: Renewable and sustainable composites, Elsevier, 1–30 (2019)
2. Al-Fatlawi, A., Jármai, K., Kovács, G.: Optimal Design of a Fiber-Reinforced Plastic Composite Sandwich Structure for the Base Plate of Aircraft Pallets In Order to Reduce Weight. Polymers **13**(5), 834 (2021)
3. Rajak, D.K., Wagh, P.H., Kumar, A., Sanjay, M.R., Siengchin, S., Khan, A.: Impact of fiber reinforced polymer composites on structural joints of tubular sections: A review ARTICLEINFO. Thin-Walled Structures **180**, 109967 (2022)
4. Dattoma, V., Nobile, R., Panella, F.W., Pirinu, A., Saponaro, A.: Damage investigation of aeronautical CFRP laminates under bearing tests. Procedia Structural Integrity **18**, 719–730 (2019)
5. Rozylo, P.: Experimental-numerical study into the stability and failure of compressed thin-walled composite profiles using progressive failure analysis and cohesive zone model. Compos. Struct. **257**, 113303 (2021)
6. Heimbs, S.: Computational methods for bird strike simulations: A review. Comput. Struct. **89**, 2093–2112 (2021)
7. Pierrat, E., Rupcic, L., Hauschild, M.Z., Laurent, A.: Global environmental mapping of the aeronautics manufacturing sector. J. Clean. Prod. **297**, 126603 (2021)
8. Allan, J.R.: The costs of bird strikes and bird strike prevention. Human Conflicts with Wildlife: Economic Considerations **1**, 147–153 (2000)

9. Monticeli, F.M., Cioffi, M.O.H., Voorwald, H.J.C.: Mode II delamination of carbon-glass fiber/epoxy hybrid composite under fatigue loading. Int. J. Fatigue **154**, 106574 (2022)
10. Monticeli, F., Fuga, F., Donadon, M.: A systematic review on translaminar fracture damage propagation in fiber-reinforced polymer composites. Thin-Walled Structures **187**, 110742 (2023)
11. Wang, F., Liu, J., Liu, L., Xu, L., Wang, Y., Chen, M.: Quantitative non-destructive evaluation of CFRP delamination defect using laser induced chirp-pulsed radar photothermal tomography. Opt. Lasers Eng. **149**, 106830 (2021)
12. Biagini, D., Pascoe, J., Alderliesten, R.: Investigating apparent plateau phases in fatigue after impact damage growth in CFRP with ultrasound scan and acoustic emissions. Int. J. Fatigue **177**, 107957 (2023)
13. Cornetti, P., Pugno, N., Carpinteri, A., Taylor, D.: Finite fracture mechanics: A coupled stress and energy failure criterion. Eng. Fract. Mech. **73**, 2021–2033 (2006)
14. Camanho, P.P., Erçin, G.H., Catalanotti, G., Mahdi, S., Linde, P.: A finite fracture mechanics model for the prediction of the open-hole strength of composite laminates. Compos. Part A Appl. Sci. Manuf. **43**, 1219–1225 (2012)
15. Roy, T., Chakraborty, D.: Delamination in hybrid FRP laminates under low velocity impact. J. Reinf. Plast. Compos. **25**, 1939–1956 (2006). https://doi.org/10.1177/0731684406069922
16. Fuga, F.R., Donadon, M.V.: Low velocity impact on pre-loaded composite plates: A novel standard-based experimental apparatus. Compos. Struct. **261**, 113315 (2021)
17. Davies, G.A.O., Zhang, X.: Impact damage prediction in carbon composite structures. Int. J. Impact Engno **16**, 149–170 (1995)
18. Yang, B., Chen, Y., Lee, J., Fu, K., Li, Y.: In-plane compression response of woven CFRP composite after low-velocity impact: Modelling and experiment. Thin-Walled Structures **158**, 107186 (2021)
19. Ramji, A., Xu, Y., Yasaee, M., Grasso, M., Weeb, P.: Influence of veil interleave distribution on the delamination resistance of cross-ply CFRP laminates under low velocity impact. Int. J. Impact Eng **157**, 103997 (2021)
20. Gutkin, R., Pinho, S.T., Robinson, P., Curtis, P.T.: A finite fracture mechanics formulation to predict fibre kinking and splitting in CFRP under combined longitudinal compression and in-plane shear. Mech. Mater. **43**, 730–739 (2011)
21. Llobet, J., Maimí, P., Essa, Y., Martin de la Escalera F. A continuum damage model for composite laminates: Part III - Fatigue. Mechanics of Materials 153, 103659 (2021)
22. Khan, R.: Fiber bridging in composite laminates: A literature review. Compos. Struct. **229**, 111418 (2019)
23. Zhang, D., Liu, L., Lan, X., Li, F., Liu, Y., Leng, J.: Experimental study on nonlinearity of unidirectional carbon fibre-reinforced shape memory polymer composites **16**, 107372 (2023)
24. Kebir, T., Benguediab, M., Imad, A.: A model for fatigue crack growth in the Paris regime under the variability of cyclic hardening and elastic properties. Fatigue of Aircraft Structures **9**, 117–135 (2017)
25. Hu, P., Pulungan, D., Tao, R., Lubineau, G.: An experimental study on the influence of intralaminar damage on interlaminar delamination properties of laminated composites. Compos. A Appl. Sci. Manuf. **131**, 105783 (2020)